Advanced Structural Mechanics 1 (2024) 56-70

Advanced Structural Mechanics

Journal homepage: https://asm.sku.ac.ir

Failure analysis of a GE-F6 Gas turbine blades

Mohsen Fatehi[a,*] , Kianoush Norouzi[b]

[a]*Rotating Equipment Expert of engineering department, NeyrPerse Co., No. 38-West Armaghan St.-Vali-e-Asr Ave., Tehran 1967843116, Iran*
[b]*Project Manager, NeyrPerse, No. 38-West Armaghan St.-Vali-e-Asr Ave., Tehran 1967843116, Iran*

Article received: 2022/04/22, Article revised: 2022/07/29, Article accepted: 2022/09/08

ABSTRACT

Gas turbines play a fundamental role in the power generation, marine, and aviation industries. The blades of gas turbines are one of the most valuable and critical parts of this type of machines. The blades' failure causes serious damage to the next stages of the turbine and compressor and may lead to long-term shut downs. In this paper, the failure of the third-stage blades of a GE-F6 gas turbine unit is studied and investigated using mechanical analysis and metallurgical experiments. The blades are made of IN-738 alloy and fail during an initial operation in the fuel change test from natural gas to liquid fuel and cause severe damage to the turbine and turbine casing. This study includes mechanical and metallurgical experiments, stress analysis by numerical methods, and analysis of recorded data from the control system during the failure time and compares them with standard data. The data are compared with those contained in the manufacturer's instructions during startup. This research shows that the blade failure occurs because of an interior object in the third stage of the turbine part, which has been separated from the turbine's blades due to the poor quality of the blades' material.

Keywords: Gas turbine; GE-Frame 6; Third Stage blades; Mechanical experiments; Numerical simulation; Stress analysis

1. Introduction

Gas turbine components are exposed to high mechanical-thermal stresses under operating conditions. The mechanical and metallurgical properties of these components undergo changes over time due to tough conditions and the application of high stress levels in gas turbine components. On the other hand, during the process of production by manufacturer, any internal metallurgical defects may occur for various reasons. These defects are either associated with the initial quality of the material or exist in the structure of the material, which can cause initial cracks or are the source of stress cracks during the part operation and increase the risk of failure. Obviously, any

* Corresponding author at: Rotating Equipment Expert of engineering department, NeyrPerse Co., No. 38-West Armaghan St.-Vali-e-Asr Ave., Tehran 1967843116, Iran
E-mail address: fatehi.mohsen1@gmail.com
DOI: 10.22034/asm.2022.13834.1003: http://asm.sku.ac.ir/article_11294.html

component failure can cause a lot of damage to the gas turbine. Following the failure of a component, several damages may occur to the gas flow path for other parts, including discs, vanes, and blades. In this situation, there will be a sudden shutdown of the turbine. Therefore, metallurgical and mechanical tests, as well as mechanical analysis to investigate the possibility of failure and identify critical areas in the blades exposed to high levels of stress are of paramount importance to determine the reasons for failure.

Jianfu Hou et al. [1] studied the blade fatigue failures using mechanical analysis of broken blades and compared laboratory results with numerical simulation using the finite element method. Lucjan [2] performed a fatigue test to investigate the possibility of failure due to blade vibrations of an air compressor. Wu [3] extensively investigated the life estimates of various materials used in gas turbine blades. Maharaj et al. [4] simulated and investigated the pine-shaped connection of the blade root and gas turbine disc to determine high-stress areas and crack modeling in those areas with the finite element method. Choi and Lee [5] also investigated the causes of blade failure by simulating the finite element method of the pine-shaped connection of the blade root in a gas turbine disc.

The studied gas turbine has a nominal output power in standard conditions equal to 42 MW. The turbine has a seventeen-stage axial flow compressor with a pressure ratio of 1:12 and a three-stage turbine mounted on a common shaft. The maximum temperature of the hot gas inlet to the first stage of the turbine in operating conditions is 1140°C, and the outlet temperature of the turbine is 548°C. The rotational speed of the turbine section in normal conditions and at full speed is equal to 5000 rpm [6,7].

When the turbine starting system is actuated, the ambient air is drawn through the air inlet plenum assembly, filtered and compressed in the 17^{th} stage of the axial flow compressor. For pulsation protection during startup, the 11^{th} stage extraction valves are open and the variable inlet guide vanes are in the closed position. When the high speed relay actuates at 95 percent speed, the 11^{th} stage extraction bleed valve is closed automatically and the variable inlet guide vane actuator is energized to open the inlet guide vanes to the normal turbine operating position. The compressed air from the compressor flows into the annular space surrounding the ten combustion chambers from which it flows into the spaces between the outer combustion casings and the combustion liners, and enters the combustion zone through metering holes in each of combustion liners.

Fuel from an off-base source is provided to ten equal flow lines, each terminating at a fuel nozzle centered in the end plate of a separate combustion chamber. Prior to being distributed to the nozzles, the fuel is accurately controlled to provide an equal flow to the ten nozzle feed lines at a rate consistent with the speed and load requirements of the gas turbine. The nozzles introduce the fuel into the combustion chambers where it is mixed with the combustion air and ignited by one or both of the spark plugs. At the moment when fuel is ignited in one combustion chamber, the flame is propagated through connecting crossfire tubes to all other combustion chambers. After the turbine rotor approximates operating speed, combustion chamber pressure causes the spark plugs to retract to remove their electrodes from the hot flame zone.

The hot gases from the combustion chambers expand into the ten separate transition pieces attached to the aft end of the combustion chamber liners and flow from there to the three-stage turbine section of the machine. Each stage consists of a row of fixed nozzles followed by a row of turbine blades. In each nozzle row, the kinetic energy of the jet is increased with an associated pressure drop, and in each following row of moving blades, apportion of the kinetic energy of the jet is absorbed as useful work on the turbine rotor.

After passing through the third-stage blades, the gases are directed toward the exhaust hood and diffuser, which contains a series of turning vanes to turn the gases from an axial direction to a radial direction, thereby minimizing exhaust hood losses. The gases then pass into the exhaust plenum and are introduced to the atmosphere through the exhaust stack. The resultant shaft rotation is used to turn the generator rotor to generate electric power or drive a centrifugal compressor in industrial power applications. Figure 1 shows the simple cycle of the gas turbine flow diagram.

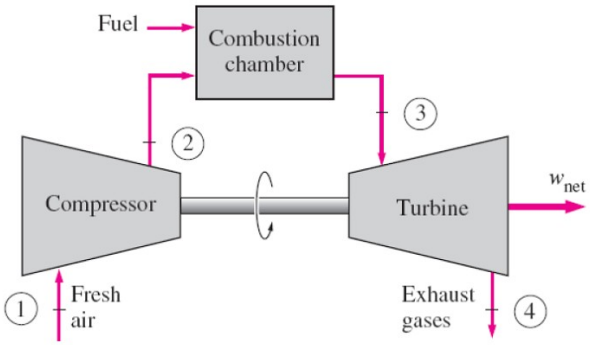

Fig. 1. Simple cycle of gas turbine flow diagram.

This turbine was started for the sixth time after 5 successful starts to test the control systems and the fuel change from natural gas to liquid fuel. After the nominal speed of 99.5% was reached, the turbine went out of operation with an abnormal sound and a high vibration of 30 inches per second. In general, the turbine has been running on natural gas fuel for 1.5 hours from the beginning of the first start until the time of the failure. In post-failure inspections and lifting of the turbine case, the vanes and blades of the third stage of the turbine were found to be severely damaged.

2. Sampling of blades' material

On this occasion, the third stage of the turbine's blades is damaged more than the other parts. In addition, the third stage vanes, as well as the shrouds of the third stage have suffered more damage than other parts of the turbine. Figure 2 shows images of the destruction of third stage blades and vanes.

For mechanical tests and metallurgical studies, the blades need to be selected. For this purpose, several parameters, including the level of destruction of the blades and their place on the stage are considered. Some blades are selected for mechanical tests and metallurgical studies according to Table 1. Blades in which part of the airfoil has been destroyed are considered broken, and blades whose airfoil has been destroyed at the root are considered completely broken. The size and shape of specimens have been sampled based on the ASTM E139 standard [8]. The numbers placed in the Tag No. column are the numbers of the blades of the third stage assigned to the blades by the manufacturer. In fact, these numbers are engraved on the blade body.

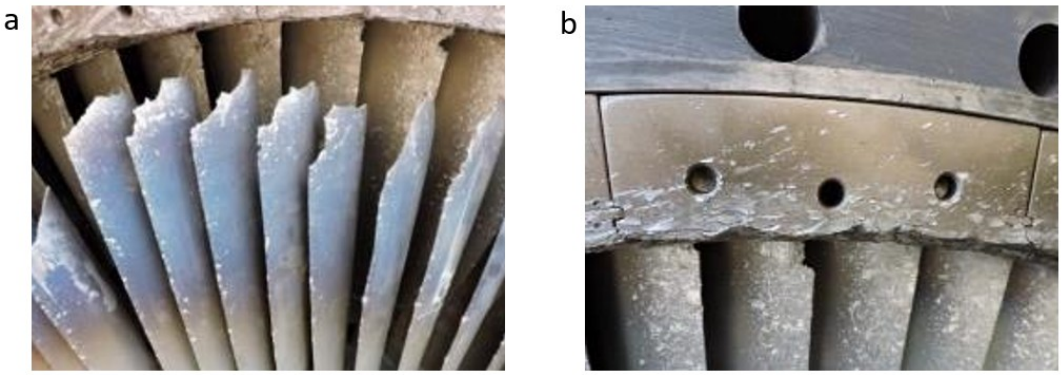

Fig. 2. (a) Destroyed blades of the third stage; (b) destroyed vanes of the third stage.

Table 1. Tag numbers and location of damaged blades on the disc.

Row	Location No.	Tag No.	Condition
1	3	D367	Broken
2	5	C672	Completely broken
3	77	B941	Broken
4	8	C680	Broken
5	12	C639	Broken
6	14	C588	Broken
7	17	C641	Broken
8	31	D319	Completely broken

3. Performed tests on the blades' material

To accurately determine the test conditions, the chemical composition of the blades is first analyzed using optical emission spectrometry. This test is performed on one of the completely broken blades (C672) and two blades from other blades (B941, D367). Based on this and according to the working conditions of the blades and based on the relevant standards, the rupture stress conditions are determined. In general, rupture stress tests are performed with temperature and stress conditions of T = 760°C and S = 562MPa, T = 815°C and S = 430MPa, T = 980°C and S = 140MPa. This test is done using a tensile stress test equipment that has a dead weight mechanism and is equipped with a three-zone furnace. In this equipment, it is possible to record the rupture stress time. The breaking stress test can be performed from a temperature of 100°C to 1200°C and up to a tensile load of 2 tons. It should be noted that this test is performed based on the ASTM E139 standard [8]. A summary of the rupture stress tests performed and the chemical analysis on the broken and completely broken blades are given in Table 2, respectively.

4. Result of tests

4.1. Chemical analysis

Emission spectrometry test is performed on blades with different codes C and D from a broken blade and a completely broken blade (C672, D367). The results of chemical analysis of the blades' material are shown in Table 3. Accordingly, the alloy of the blades in terms of the main elements corresponds to the chemical composition in the technical specifications of ALLOY IN-738 INCO-IN-738LC [9].

Table 2. Summary of the test performed on the blades' material.

Row	Tag No.	Test
1	C588	Rupture stress at 760°C and 562 MPa stress on root
2	C639	Rupture stress at 760°C and 562 MPa stress on airfoil
3	D367	Rupture stress at 815°C and 430 MPa stress on root
4	C641	Rupture stress at 815°C and 430 MPa stress on airfoil
5	C641	Rupture stress at 980°C and 140 MPa stress on root
6	C680	Rupture stress at 980°C and 140 MPa stress on airfoil
7	C672	Emission spectrometry
8	D367	Emission spectrometry

Table 3. Results of chemical analysis of blades using emission spectrometry.

Tag No	Element	Weight percent	Tag No	Element	Weight percent
	Carbon	0.13		Carbon	0.10
	Cobalt	8.34		Cobalt	8.68
	Chromium	16.1		Chromium	15.70
	Molybdenum	1.50		Molybdenum	1.50
	Tungsten	2.70		Tungsten	2.80
	Tantalum	1.70		Tantalum	1.72
	Columbium (Niobium)	0.63		Columbium (Niobium)	0.61
	Aluminum	3.60		Aluminum	3.60
C672	Titanium	3.21	D367	Titanium	3.20
	Aluminum+ Titanium	6.80		Aluminum+ Titanium	6.50
	Boron	0.01		Boron	0.009
	Zirconium	0.05		Zirconium	0.04
	Iron	0.06		Iron	0.13
	Manganese	<0.001		Manganese	<0.001
	Silicon	0.03		Silicon	0.03
	Sulfur	0.009		Sulfur	0.005
	Nickel	61.88		Nickel	61.81

4.2. Rupture stress test

The rupture stress test has been performed on the blades' roots and airfoils at 760°C, 815°C, and 980°C according to the standard [8]. Comparison of rupture stress diagrams in terms of failure time of airfoil samples and blades' root at 760°C, 815°C, and 980°C are shown in Fig. 3., respectively. According to the technical specifications of ALLOY IN-738 INCO-IN-738LC [9] and the relevant standards [8], the alloy of the blade must be able to withstand temperature and stress conditions of T = 760˚C and S = 562 MPa, T = 815˚C and S = 430 MPa, T = 980˚C and S = 140 MPa for 100 hours. More than 70% of the samples failed in less than 100 hours, while the minimum stress has been considered for different temperatures [8].

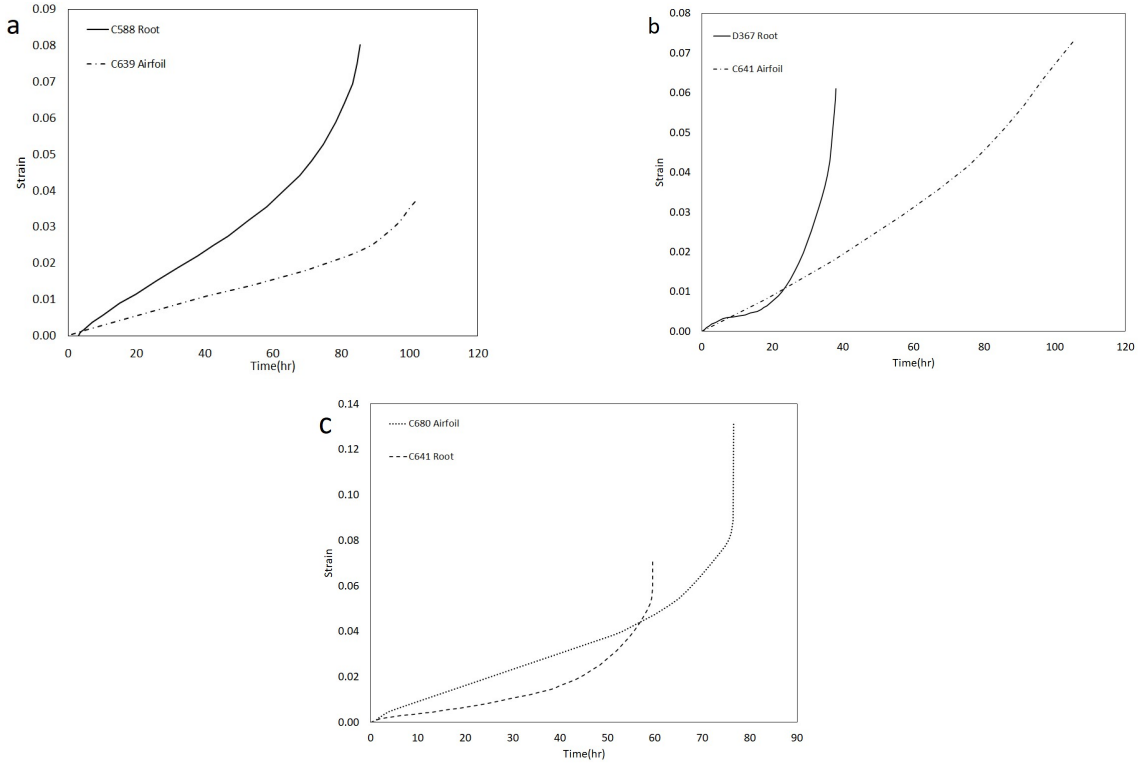

Fig. 3. Comparison of rupture stress diagrams of samples prepared from blades in (a) Temperature of 760°C; (b) Temperature of 815°C; (c) Temperature of 980°C.

5. Numerical Simulation of hot gas flow around the airfoil

The flow of hot gas passing through the blades puts pressure on the blades' surfaces that is not the same in different sections. In this section, the hot gas flow on the blade is modeled according to the modeling of the third stage blade profile and the selection of the appropriate domain of the hot gas flow, as well as the use of flow quantities and boundary conditions recorded by the control system when the failure occurs by the ANSYS workbench using the module of CFX. The purpose of this simulation is to calculate the compressive and temperature stresses generated on the blade airfoil and use it to analyze the final blade stress. The blade geometry is modeled in three dimensions using the actual GE-F6 turbine's third-stage turbine blade. Also, the domain of hot gas flow related to each blade is considered according to the distance of the blades from each other. The third stage of the GE-F6 turbine has 92 blades. Figure 4 shows the geometry of the blade and the domain of hot gas flow. The inlet hot gas flow with an appropriate approximation of the third stage vanes of this turbine is considered to be 53 degrees relative to the vertical flow. The simulation of the first and second stages of the turbine has been omitted in order to prevent the increase of the calculation volume.

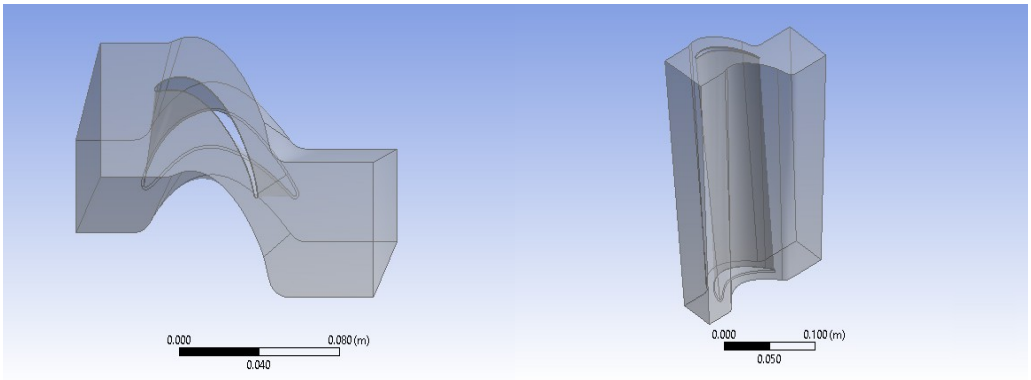

Fig. 4. Domain of the hot gas flow in the turbine's third stage blades.

5.1. Governing equations and modeling of turbulent flow

The Reynolds-averaged Navier-Stokes equations for incompressible flows are the main governing equations, which may be written as Eq. (1) and Eq. (2) [10].

$$\frac{\partial \bar{u}_i}{\partial x_i} = 0 \tag{1}$$

$$\rho\left(\frac{\partial \bar{u}_i}{\partial t} + \bar{u}_j \frac{\partial \bar{u}_i}{\partial x_j}\right) = \bar{B}_i - \frac{\partial \bar{p}}{\partial x_i} + \frac{\partial}{\partial x_j}\left(\mu \frac{\partial \bar{u}_i}{\partial x_j} - \rho \overline{u_i' u_j'}\right) \tag{2}$$

Where u_i is the fluid mean velocity, p is the mean pressure, v is the fluid kinematic viscosity, and $\bar{B}_i$ is the mean body force. The apparent extra stress term on the right-hand side of the momentum equation, $\rho u_i' u_j'$ is referred to as the Reynolds stress, and should be modeled via an appropriate turbulence model.

In this study, the turbulent flow model of shear stress transport has been used to simulate the hot gas flow passing through the blade. This model is a hybrid of *k-ω* and *k-ε* models, so that the *k-ω* model is used in the parts inside the boundary layer and the *k-ε* model is used in the parts outside the boundary layer. To better explain this model, an F1 function is introduced that is equal to one near the wall and zero outside the boundary layer and away from the wall. Based on this function, the *k-ω* model will be activated near the wall and the *k-ε* model will be activated in other parts of the flow [11].

5.2. Meshing and grid steady of hot gas flow domain

The domain of the hot gas flow is considered from the third stage vane outlet to the turbine's exhaust, where the gas exits from the turbine. Surface grids are made using hexahedral meshes. Using the mesh control tools on the surface, the number of meshes on the wall and in the parts where the y^+ in the boundary layer of the flow is low has been made sufficiently fine. Figure. 5. shows how the meshes are generated in the domain of hot gas flow and in the tip and root near the blade wall. As shown in the picture, an attempt has been made to make the meshes fine enough for the tip and root regions of the blade.

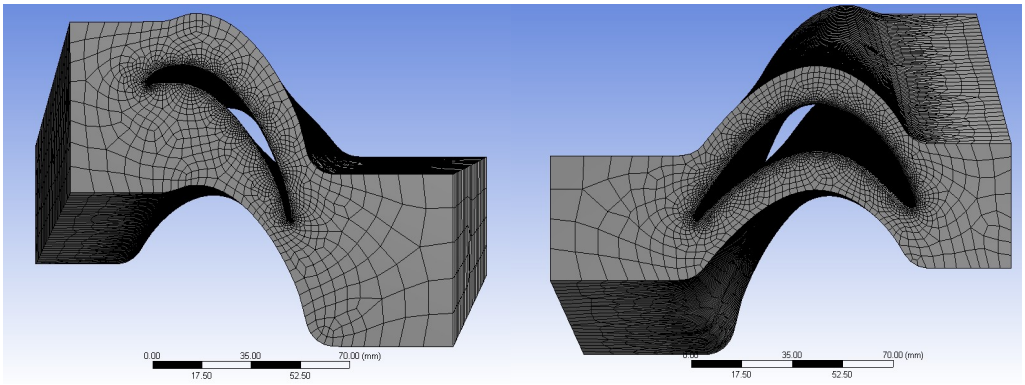

Fig. 5. Meshing for the domain of hot gas flow in the third stage turbine's blade.

To investigate the independence of the results from the elements number of meshing in this case, meshing with the number of elements 1,234,973, 1,852,459, and 2,778,689 have been created, and the results of the last two meshing show independence of the results from the number of elements. Table 4 presents the grid steady for the value of the minimum and maximum pressure and temperature on the blade wall for the number of elements generated.

5.3. Boundary conditions

Boundary conditions used to solve this problem are the mass flow rate and the output pressure which is shown in Eq. (3) to Eq. (8) Local atmospheric conditions on the day of the accident are as follows.

$$P_a = 1.017 \text{ bar} \tag{3}$$

$$T_a = 35^\circ C = 308K \tag{4}$$

Boundary conditions at the inlet and outlet of the third stage blades of the turbine are as follows:

$$\dot{m}_{inlet} = 145\ kg/s \tag{5}$$

$$T_{inlet} = 400^\circ C = 673K \tag{6}$$

$$P_{outlet} = 1.027bar = P_a + 10mbar \tag{7}$$

$$T_{outlet} = 300^\circ C = 573K \tag{8}$$

Table 4. Grid steady for temperature and pressure.

Row	Item	Number	Quantity	Maximum	Minimum
1	Node	770,222	Temperature (K)	490.1	727.6
	Cell	1,234,973	Pressure (MPa)	-139.6	212.4
2	Node	1,155,333	Temperature (K)	494.2	724.5
	Cell	1,852,459	Pressure (MPa)	-118.9	216.8
3	Node	1,733,000	Temperature (K)	494.8	752.2
	Cell	2,778,489	Pressure (MPa)	-118.9	217.1

The rotational speed of the turbine is 5080 rpm and based on the equation of burning methane gas with air Eq. (9), the composition of the fluid passing through the blade can be obtained.

$$CH_4 + 2\times(3.7N_2 + O_2) \rightarrow CO_2 + 2H_2O + 2\times 3.7N_2 \tag{9}$$

According to Eq. (16), the fluid passing through the blade can be determined as a combination of CO2, N2 and H2O (water vapor).

5.4. Results of hot gas numerical simulation

Due to the importance of compressive and temperature stresses in the blade and in order to simulate the condition of the blade when the turbine is operating at full speed-no load state, the temperature and fluid pressure distribution around the blade are simulated and shown in this section.

Figure 6 shows the temperature distribution in the blade wall. The temperature distribution contour on the blade indicates that the maximum steady-state temperature is 730.4 K. The temperature distribution is such that the lower part of the blade has a temperature of about 648 K and the temperature increases along the longitudinal axis of the blade. The graph of the average temperature increase along the blade is shown in Fig. 7.

Figure 8 shows the fluid pressure distribution on the blade wall. The pressure distribution in the blade wall indicates that the maximum pressure at the blade leading edge is 0.2 MPa. Also the pressure in the front area of the blade has an average value of about 0.06 MPa, and the pressure changes from the root to the tip have an increasing trend, which is shown in Fig. 9 (a). Figure 9 (b) shows the trend of changes in the average hot gas pressure from the

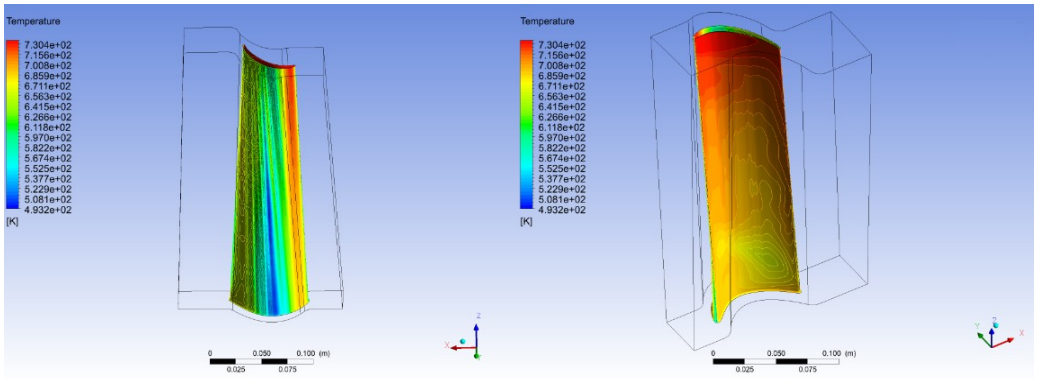

Fig. 6. Hot gas temperature distribution on the wall of the third stage blade.

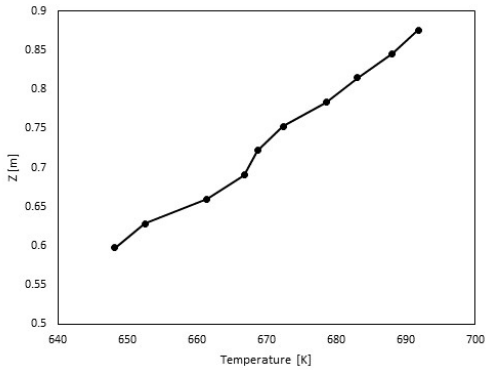

Fig. 7. Changes in the average hot gas temperature on the blade's wall from root to tip.

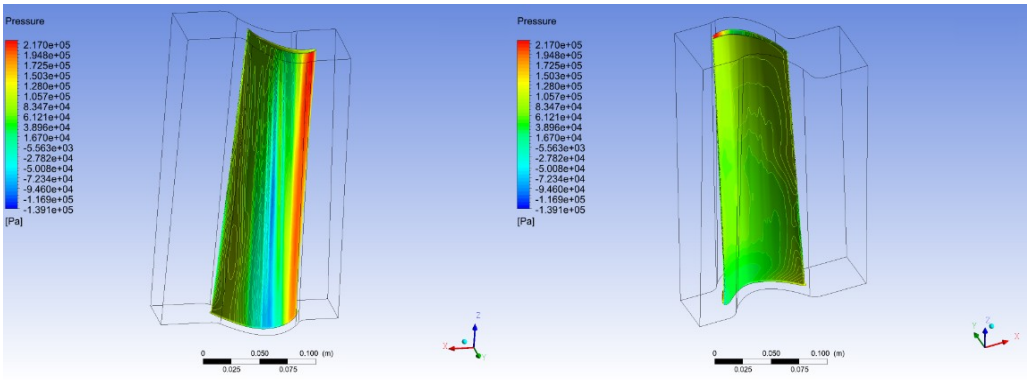

Fig. 8. Hot gas temperature distribution on the wall of the third stage blade.

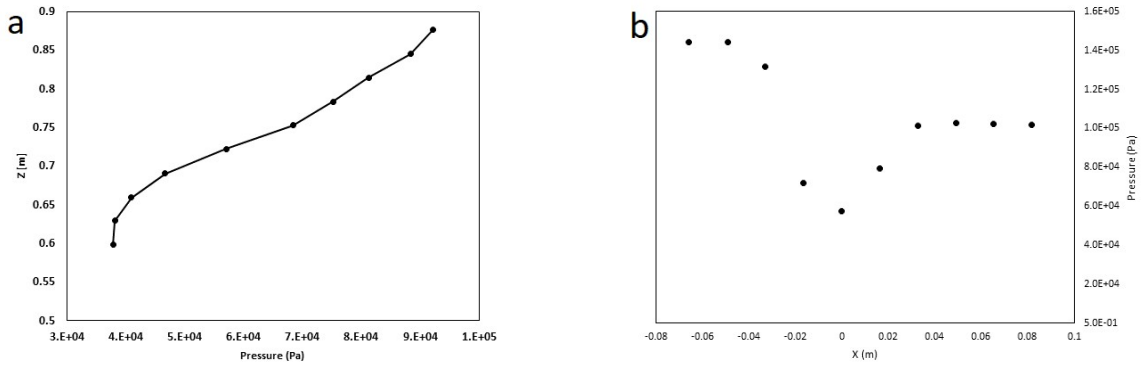

Fig. 9. Changes in the average hot gas pressure on the blade wall (a) from root to tip, (b) from inlet to Outlet.

inlet and after passing through the blade to the outlet which is discharged to the exhaust. As can be seen in this diagram, the fluid flow at the inlet has a pressure of 0.145 MPa and it is discharged to the exhaust after a sudden pressure drop of about 0.09 MPa when it passes through the blade, and at the outlet its pressure is more than 0.1 MPa which is equal to the local air pressure.

6. Stress analysis of the blade

6.1. Blade material and physical properties

According to the turbine manufacturer's standard [12], the blade is made of IN-738 alloy, which is a kind of nickel-based super alloy. The physical properties of this alloy can be seen in Table 5. Due to the significant influence of the physical properties of the blade on stress calculations, the metallurgical and physical properties of the alloy have been fully entered into the ANSYS workbench engineering data.

6.2. 3D modeling of blade geometry

The 3D geometry of the third-stage blade is modeled according to the actual airfoil, considering the root of the blade, shroud at top of the blade, and the modeling of the disc-related segment as shown in Fig. 10. The blade input model for analysis is the actual blade model. The exact same model is used to make the blade, which is an accurate

Table 5. Physical properties of IN-738 alloy.

K (W/M K)	E (GPa)	A	C (J/Kg K)	V	S_y (MPa)	S_{ut}(Mpa)
23.5	200	$11.6*10^{-6}$	420	0.29	690	895

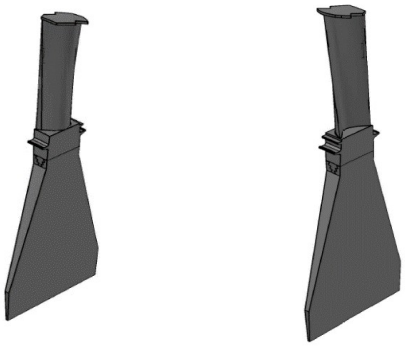

Fig. 10. Third stage blade and disc segment geometry, the front and rear view.

casting method. Usually, in complex geometric models, simplifications are performed on it to the extent that it does not significantly affect the results of the analysis, but in this study, in order to perform better analysis and to achieve higher result accuracy, no simplifications are made on the 3D model of the blade. The blade has three parts: root, airfoil and shroud. In the blade, all surfaces of the pressure and suction side, the lead edge, and the trailing edge are significant from a stress point of view. The blade's root is pine-shaped, which connects and fastens the blade to the disc.

6.3. Boundary condition

As the boundary condition, for simplification, it is assumed that the blade is fixed inside the disc and has a degree of freedom only in the direction of rotation around the rotor axis, which is compatible with the actual conditions of the blade and disc structural support. Therefore, the blade has no degrees of freedom in the three main directions of Cartesian coordinates xyz and also rotation around the x and y axes. It has a rotation only around the rotor axis and has a degree of freedom around the z-axis.

6.4. Temperature, pressure and initial conditions in steady-state

In this section, the results of mechanical-thermal stress analysis for the third-stage blade of the turbine with mechanical properties of the nickel-based alloy of IN-738 at full speed-no load at a steady-state are presented. This analysis has been done by the ANSYS workbench using the module of static structural mechanics. In performing these analyses, the steady-state pressure and temperature at 100% speed are applied to the three-dimensional blade model. Also, the rotational speed, according to the recorded data, is equal to 5080 rpm for the turbine. It is noticeable that since the start of the gas turbine, it has taken about 1000 seconds for the rotor to reach the mentioned rotational speed, and then the stresses in the rotation of the blade reach the steady-state after 1600 seconds. At this time, the blade reaches its maximum operating temperature at the steady-state.

Considering the blade material and its physical properties, the blade temperature in operation conditions can impose certain thermal stresses on the blade body. For better analysis of blade temperature, data of fluid temperature on the blade wall have been used, which is the result of hot gas simulation around it (section 5-4). Moreover, for simulation by finite element method, the stress analysis in the steady-state is assumed to ignore the temperature gradient between the blade and the disc. This assumption is due to the fact that the existence of a contact boundary condition (the distance between the swallowtail root and the pine-shaped root of the disc) in finite element analysis creates a temperature gradient between the blade and the disc, which causes an almost significant temperature difference in the contact point. To avoid this situation, which is only due to the solution error in the finite element solution method, it is assumed that heat transfer is just from the blade to the disc and there is not any heat transfer from the disc side to the blade. In addition, the flow of hot gas passing through the blade creates a pressure on the blade surface that is not the same at different sections of the blade. This pressure, which is actually the cause of the

blade rotation around the rotor axis, has been calculated according to the solution of the fluid flow around the blade and applied to the blade (section 5-4).

6.5. Meshing and grid steady of the blade

To check the grid steady, three different types of meshing have been used in terms of size and number of elements. Therefore, by comparing these three types of meshing, the independence of the results can be checked. Checking the results presented in Table 6, it can be seen that the maximum difference between the equivalent stresses in the last two types of meshing is about 7 MPa, i.e., approximately 0.3% of the total equivalent stress. This case indicates the convergence of the solution by the finite element method. All three types of meshing, with an acceptable approximation, show the amount of equivalent stress on the blade. The third type of meshing has been used in the analysis. Figure 11 shows the blade's meshing.

6.6. Results of stress analysis for the blade

Figures 12 and 13 show the equivalent stress distribution in the blade and the contact area of the blade's root and disc, respectively. This result is obtained from structural analysis by applying the distribution of temperature, pressure, and rotation at 100% speed in the third stage of the turbine's blade. The maximum amount of equivalent stress is 2258 MPa which occurs in the contact zone of the disc and blade, and the highest amount of equivalent stress in the blade's airfoil, where the failure occurs, is in the tip of the blade, and equals 702 MPa. According to the temperature distribution on the blade in section 5-4, the temperature value in this part of the blade's tip, with the highest amount of equivalent stress, is about 460°C.

Table 6. Grid steady for equivalent stress.

Row	Item	Number	Quantity	Maximum	Minimum
1	Node Cell	113,559 65,506	Equivalent stress (MPa)	0.55	2215.4
2	Node Cell	170,392 98,295	Equivalent stress (MPa)	0.49	2251.3
3	Node Cell	255,589 147,389	Equivalent stress (MPa)	0.41	2258.1

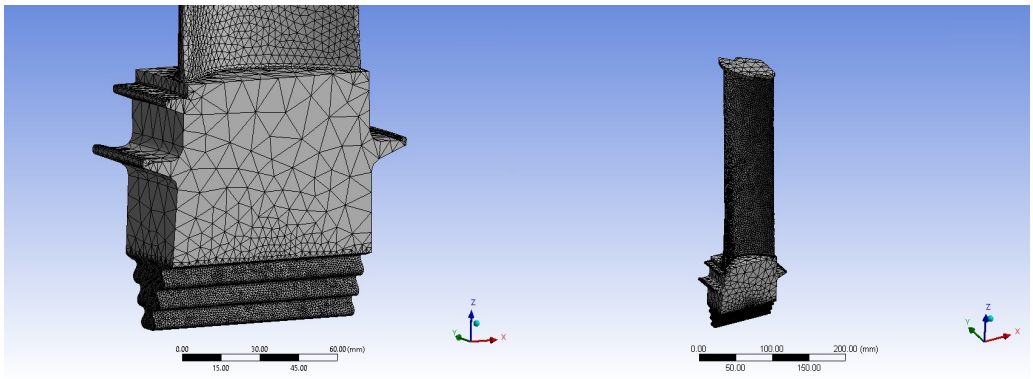

Fig. 11. Meshing of the blade.

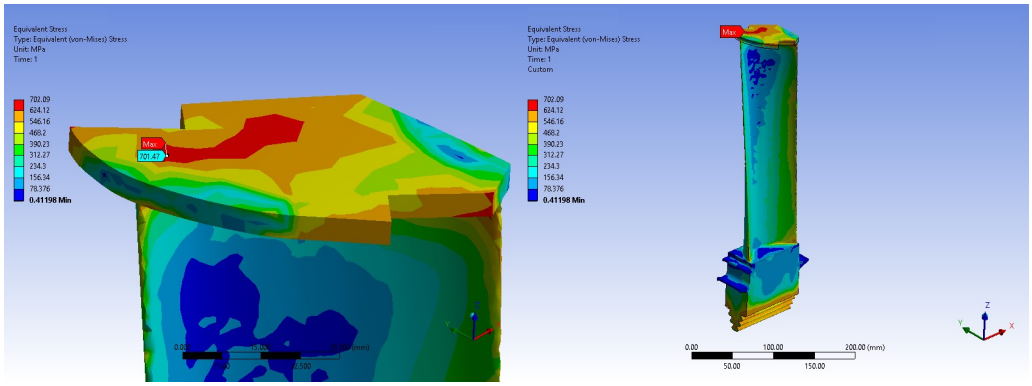

Fig. 12. Equivalent stress (Von Mises) distribution on the third stage blade of the turbine.

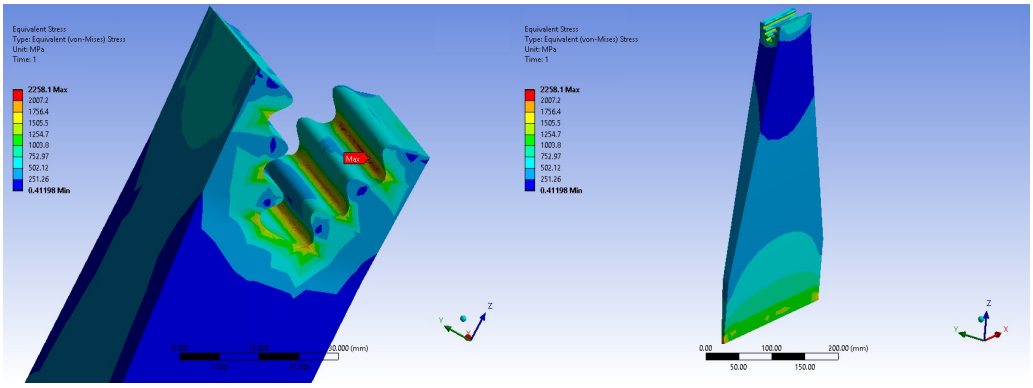

Fig. 13. Equivalent stress (Von Mises) distribution on the third stage disc of the turbine.

Figure 14 shows the deformation in the z-direction or the increase in blade length in this direction. The blade increases in length due to exposure to high temperatures and the presence of centrifugal force. Deformation in the x and y directions has been omitted, due to its small size and only the increase in length in the z-direction has been investigated. As can be seen in Fig. 14., the maximum increase in length is 4.37 mm, which occurs at the blade's tip, and due to the low temperature in the root of the blade, the lowest length increase occurs in this part. Investigation of blade length increase is important because the assumption that the blade tip collides with the shroud due to the increase in length can be checked. This can be one of the reasons for blade failure. Considering the amount of increase in length obtained in this analysis (4.37 mm), and comparison with the allowable tolerances in the turbine manufacturer's documents [7], which in the third stage has the allowable tolerance of 6.21±0.5 mm between the blade tip and the honeycomb shroud section, it can be concluded that the collision of the tip of the blade with the shroud is not the reason for the failure of the blade.

Figure 15 also shows the elastic strain distribution in the blade. The maximum amount of strain is at the blade's tip and equals 0.0042. Comparing this value with the results obtained from the rupture stress test (section 4-2), it is observed that the amount of strain of this blade is much less than the values obtained for the blade's material under the test by considering IN-738 in standard conditions and standard turbine operating conditions at steady-state temperature and pressure.

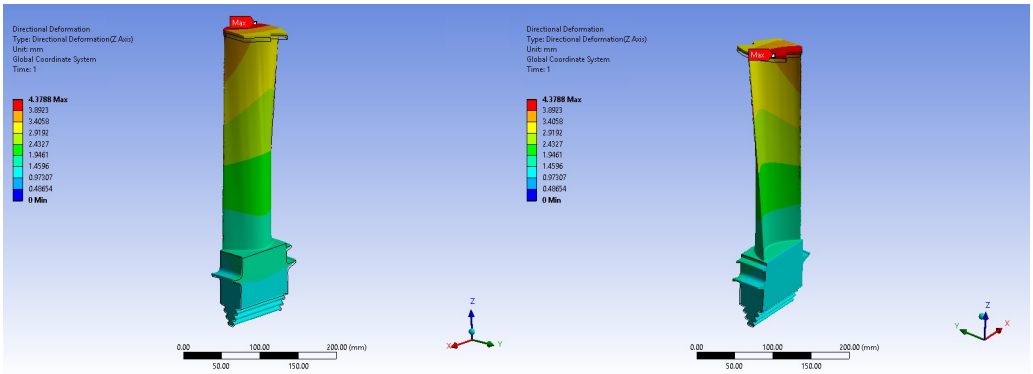

Fig. 14. Deformation in the z-direction of the third stage of the turbine's blade.

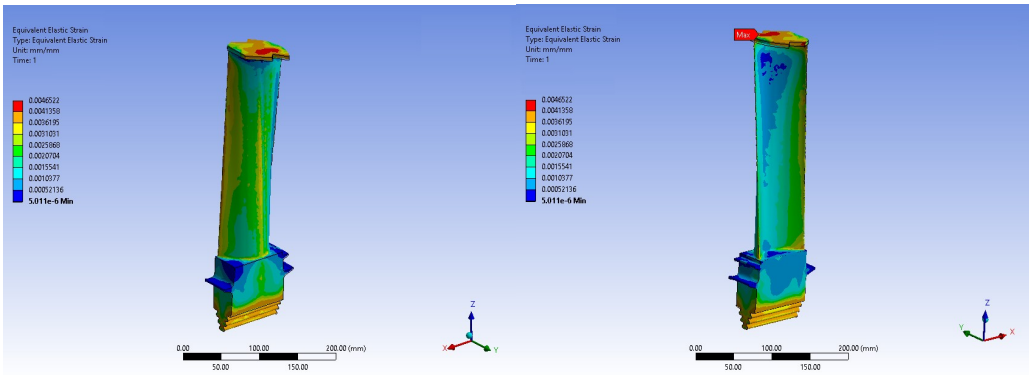

Fig. 15. Elastic equivalent strain of the third stage of the turbine's blade.

7. Conclusion

In this research, the broken blades of the third stage of a gas turbine were numerically simulated with real data. The fluid analysis simulation examined the temperature, pressure, and stresses distributions on the blades. Also, at the same time, mechanical tests were performed on them. Despite the fact that in the previous literature, various issues have been investigated regarding the reasons for the failure of the gas turbine blades, this work is unique because it has examined the numerical and experimental analyses simultaneously and used the real data during the operation of the turbine. Since the destruction of the turbine blades occurred only in the third stage, experimental investigations and numerical analysis were performed only for the blades of this stage. According to the numerical simulation performed in two parts of hot gas flow simulation around the third stage blades of the turbine and the simulation of stresses in the third stage blades, this analytical study found that the maximum stresses on the blade according to the blade temperature is much lower than the stresses that standard material of IN-738 can withstand. Also, considering the strain obtained from this analysis, it can be concluded that the strain of the blade with the properties of the mentioned material is much less than the actual strain of the blade, which has been tested for rupture stress. Finally, the assumption of the blade tip collision with the shroud can be violated by comparing the maximum increase in blade length with the manufacturer's standard tolerances. Because the increase in blade length at its maximum is less than the standard blade tip tolerance from the shroud in the manufacturer's documents [7].

Based on the tests and analyses performed, the cause of the failure can be investigated in the following two cases:

- Existence of an exterior object. The occurrence of this phenomenon can be justified in a situation where its implications can be seen before the third stage, for example, in the first and second stages of the turbine, while the damage to the turbine is seen only in the third stage.

- Existence of an interior object. This means that an object is separated from the vanes or blades of the third stage. The smallest separated object during installation or operation can cause this damage.

  According to the explanations given, it is concluded that the failure occurs due to the presence of an interior object. Accordingly, the damaged blades' material does not meet the requirements of the relevant standards. The results of the blade in the rupture stress test also show that despite the blades being subjected to the amount of rupture stress within the standard allowable range, their roots have low mechanical properties. Therefore, it can be claimed that these blades have failed due to their low-quality mechanical properties. In other words, if the blades of the third stage installed on the turbine have standard material characteristics the failure does not. However, as the materials related to these blades cannot pass the mechanical tests, it is clear that the materials used in their construction have low quality. As a result, the failure of these blades can be attributed to deformation exceeding the standard, which causes the blades to collide with the shroud, or it fails without the blade hitting other components because it cannot withstand the imposed stresses, and fatigue occurs.

References

[1] Jianfu, H., Bryon, J.W., Ross, A.A., 2002. An investigation of fatigue failures of turbine blade in a gas turbine engine by mechanical analysis. Engineering Failure Analysis. 9(2), 201–211.
[2] Lucjan, W., 2009. Experimental crack propagation analysis of the compressor blades working in high cycle fatigue condition. Engineering Failure Analysis. 16(7), 2163–2170.
[3] Wu, X., 2010. Life prediction of gas turbine materials. Institute for Aerospace Research, National research Council, Canada., pp.215–283.
[4] Maharaj, Y. C., Morris, A., Dear, J. P., 2012. Modeling of creep in inconel 706 turbine disc fir-tree. Materials Science and Engineering. 558, 412–451.
[5] Choi, Y. S., Lee, K. H., 2010. Investigation of blade failure in a gas turbine. Journal of Mechanical Science and Technology. 24, 1969–1974.
[6] Ginter, T., Carbos, O., 2010. Uprate Options for the MS6001 Heavy Duty Gas Turbine. GER-4217B, GE Energy Service.
[7] GE Energy Service., GT system description & operation. MS6001 GT, Vol. 7.
[8] ASTM E139-11.,2011. INC., Standard Test Methods for Conducting Creep, Creep-Rupture, and Stress Rupture Tests of Metallic Materials.
[9] The International Nickel Company., INC., ALLOY IN-738 Technical Data. One New York Plaza, New York, N.Y. 10004.
[10] Hozhabr, A., Tahavvor, A., Samimi, S., 2012. Numerical simulation of flow field between gas turbine blades GE F9 model. 4th Conference on Thermal Power Plants. 1–5.
[10] Alfonsi, G., 2009. Reynolds-Averaged Navier–Stokes equations for turbulence modeling. Transactions of the ASME. 62, 040802.
[11] Menter, F., Ferreira, J.C., Esch, T., Konno, B., 2003. The SST turbulence model with improved wall treatment for heat transfer predictions in gas turbines. Proceedings of the international gas turbine congress., 2–7.
[12] GE Energy Service., GT system description & operation. MS6001 GT, Vol. 8.